REFERENCES

1. D.R. Smith, W.J. Padilla, D.C. Vier, S.C. Nemat-Nasser, and S. Schultz, Composite medium with simultaneously negative permeability and permittivity, Phys Rev Lett 84 (2000), 4184–4187.

2. S. Enoch, G. Tayab, and P. Vincent, A metamaterial for directive emission, Phys Rev Lett 89 (2002), 3901–3904.

3. K. Alici and E. Ozbay, Radiation properties of a split ring resonator and monopole composites, Phys Status Solidi B 244 (2007), 1192–1196.

4. N.I. Landy, S. Sajuyigbe, J.J. Mock, D.R. Smith, and W.J. Padilla, Perfect metamaterial absorber, Phys Rev Lett 100 (2008), 207402.

5. A. Noor and Z. Hu, Metamaterial dual polarised resistive Hilbert curve array radar absorber, IET Microwave Antennas Propag 4 (2010), 667–673.

6. J. Hao, J. Wang, X. Liu, W.J. Padilla, L. Zhou, and M. Qiu, High performance optical absorber based on a plasmonic metamaterial, Appl Phys Lett 96 (2010), 251104.

7. B.R. Bian, S.B. Liu, S.Y. Wang, X.K. Kong, Y.N. Guo, and X. Zhao, Cylinderical optimized nonmagnetic concentrator with minimized scattering, Opt Express 21 (2013), 231–240.

8. S.A. Cummer, B.I. Popa, D. Schurig, D.R. Smith, and J.B. Pendry, Full wave simulations of electromagnetic cloaking structures, Phys Rev Lett E 74 (2006), 036621.

9. D. Schurig, J.J. Mock, B.J. Justice, S.A. Cummer, J.B. Pendry, A.F. Starr, and D.R. Smith, Metamaterial electromagnetic cloak at microwave frequencies, Science 314 (2006), 977–980.

10. H. Tao, N.I. Landy, C.M. Bingham, X. Zhang, R.D. Averitt, and W.J. Padilla, A metamaterial absorber for the terahertz regime: Design, fabrication and characterization, Opt Express 16 (2008), 7181–7188.

11. H. Tao, C.M. Bingham, A.C. Strikwerda, D. Pilon, D. Shrekenhamer, N.I. Landy, K. Fan, X. Zhang, W.J. Padilla, and R.D. Averitt, Highly flexible wide angle of incidence terahertz metamaterial absorber: Design, fabrication, and characterization, Phys Rev B 78 (2008), 241103.

12. N.I. Landy, C.M. Bingham, T. Tyler, N. Jokerst, D.R. Smith, and W.J. Padilla, Design, theory, and measurement of a polarization-insensitive absorber for teraherz imaging, Phys Rev B 79 (2009), 125104–125109.

13. S. Ghosh, S. Bhattacharyya, Y. Kaiprath, and K.V. Srivastava, Bandwidth enhanced polarization-insensitive microwave metamaterial absorber and its equivalent circuit model, J Appl Phys 115 (2014), 104503.

14. S. Bhattacharyya and K.V. Srivastava, Triple band polarization-independent ultra-thin metamaterial absorber using electric field-driven LC resonator, J Appl Phys 115 (2014), 064508.

15. J. Lee and S. Lim, Bandwidth enhanced and polarisation insensitive metamaterial absorber using double resonance, Electron Lett 47 (2011), 8–9.

16. S. Ghosh, S. Bhattacharyya, and K.V. Srivastava, Bandwidth-enhancement of an ultrathin polarization insensitive metamaterial absorber, Microwave Opt Technol Lett 56 (2014), 350–355.

17. S. Bhattacharyya, S. Ghosh, and K. V. Srivastava, Triple band polarization-independent metamaterial absorber with bandwidth enhancement at X-band, J Appl Phys 114 (2013), 094514.

18. M. Yoo and S. Lim, Polarization independent and ultra-wideband metamaterial absorber using a hexagonal artificial impedance surface and a resistor-capacitor layer, IEEE Trans Antennas Wireless Propag 62 (2014), 2652–2658.

19. S. Ghosh, S. Bhattacharyya, D. Chaurasiya, and K.V. Srivastava, An ultra-wideband ultra-thin metamaterial absorber based on circular split rings, IEEE Antennas Wireless Propag Lett 14 (2015), 1172–1175.

20. S. Ghosh, S. Bhattacharyya, D. Chaurasiya, and K.V. Srivastava, Bandwidth-enhanced dual-band dual-layer polarization-independent ultra-thin metamaterial absorber, J Material Science & Processing, Appl Phys A 118 (2014), 207–215.

21. H. Xiong, J.S. Hong, C.M. Luo, and L.L. Zhong, An ultrathin and broadband metamaterial absorber using multi-layer structures, J Appl Phys 114 (2013), 064109.

22. A.Y. Wang, S.B. Liu, B.R. Bian, Z.W. Mao, X.C. Liu, B. Ma, and L. Chen, A novel ultrathin and broadband microwave metamaterial absorber, J Appl Phys 116 (2014), 094504.

23. H.M. Lee and H.S. Lee, A metamaterial based microwave absorber composed of coplanar electric-field-coupled resonator and wire array, Prog Electromagn Res C 34 (2013), 111–121.

A NOVEL COMBINATORIAL TRIANGLE-TYPE AMC STRUCTURE FOR RCS REDUCTION

Tao Hong,[1] Han Dong,[1] Jun Wang,[2] Huansheng Ning,[3] Yuan Wei,[1] and Lingfeng Mao[3]
[1] School of Electronic and Information Engineering, Beihang University, Beijing 100191, China
[2] Beijing Electro-Mechanical Engineering Institute, Beijing 100074, China
[3] School of Computer and Communication Engineering, University of Science and Technology Beijing, Beijing 100083, China; Corresponding author: ninghuansheng@ustb.edu.cn
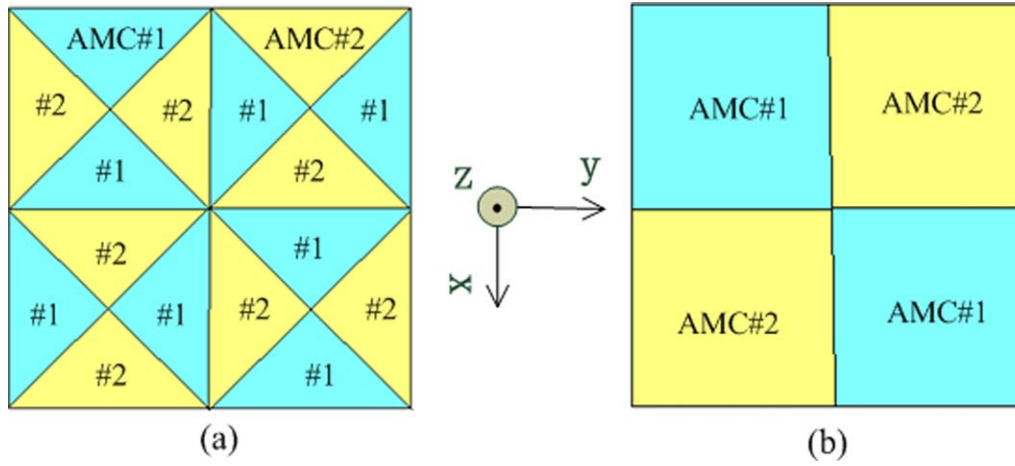
ABSTRACT: *A novel combinatorial triangle-type artificial magnetic conductor (AMC) structure for radar cross section (RCS) reduction is presented in this article. The AMC part in conventional chessboard configuration is replaced with four triangle-type AMC parts, so that the power can be transferred into more directions leading to the peak scattered field reduction. A simplified model is constructed to analyze the behavior of the proposed structure. The simulated results show that the peak value is reduced by more than 5 dB compared with the conventional chessboard configuration and the bistatic RCS is below −10 dB in a wide angular range from theta = −25° to 25°. Moreover, measurement of the monostatic RCS for the proposed structure is also conducted.* © 2015 Wiley Periodicals, Inc. Microwave Opt Technol Lett 57:2728–2732, 2015; View this article online at wileyonlinelibrary.com. DOI 10.1002/mop.29427

1. INTRODUCTION

Electromagnetic metamaterials composed of subwavelength structures can achieve extraordinary physical properties which are not possible for natural material, such as a negative index of refraction [1], electromagnetic band-gap [2], or artificial magnetic conductor (AMC) [3–6]. An AMC acts as a magnetic conductor over a certain frequency range and exhibits a reflectivity of +1 [3]. Due to this unique characteristic, AMC plays an important role in the radar cross section (RCS) reduction [7–13].

In [11], the RCS reduction is obtained by combining AMC and perfect electric conductor (PEC) parts in a chessboard configuration. The working principle of this method is to make the reflected waves produced by AMC and PEC parts interference destructively. However, the bandwidth of 10-dB RCS reduction is quite narrow. To improve the bandwidth, the PEC cells are substituted by another AMC cells operated at a different operated frequency. Using the effective phase differential between two different AMC cells, the bandwidth are significantly increased and can be more than 40% as demonstrated in [13,14]. As the abovementioned chessboard configuration has no lossy component, the power is not absorbed but transferred to other directions. For the chessboard configuration, the power is mainly scattered in the diagonal direction and the peak value of bistatic RCS is relatively high, which is harmful for target stealth.

Figure 1 Unit cell of the proposed combinatorial triangle-type AMC structure (a) and conventional chessboard structure. [Color figure can be viewed in the online issue, which is available at wileyonlinelibrary.com]

To reduce the peak scattered field of conventional chessboard structure, a combinatorial triangle-type AMC structure for RCS reduction is presented in this article. Through the combinatorial triangle-type configuration, the power may be redirected in more directions. Thus, the maximum value of the scattered field can be attenuated due to the decentralized distribution of power. A simplified model is developed to analyze the behavior of the proposed structure. Simulation and measurement of the proposed structure are also implemented to demonstrate its performance for RCS reduction.

2. OPERATION PRINCIPLE OF THE PROPOSED STRUCTURE

The working principle for RCS reduction is to design a surface that manipulates the impinging incident wave with different phase at the same time. This can be achieved by proper combination of AMC parts. Figure 1(a) shows the unit cell of the proposed combinatorial triangle-type AMC structure. Compared with the chessboard configuration depicted in Figure 1(b), the conventional AMC part is replaced with four triangle-type AMC elements. The unit cell of the proposed structure can be modeled as an antenna array formed by 16 elementary antennas. Thus, the radiated field of each AMC element is represented by

$$\vec{E}_{\text{AMC\#1}} = A_1 e^{j\varphi_1} \vec{E}_{\text{element}}, \ \vec{E}_{\text{AMC\#2}} = A_2 e^{j\varphi_2} \vec{E}_{\text{element}} \quad (1)$$

where φ_1 and φ_2 are the phase change caused by the AMC 1 and AMC #2, A_1 and A_2 are the amplitude change of two AMC elements.

The total radiated field of the array is then given as:

$$\vec{E} = \vec{E}_{\text{AMC1}} \cdot \text{AF}_1 + \vec{E}_{\text{AMC2}} \cdot \text{AF}_2 \quad (2)$$

where the antenna array factor AF_1 and AF_2 are described as:

$$\text{AF}_1 = e^{j(\psi_x/4 + \psi_y/2)} + e^{j(3\psi_x/4 + \psi_y/2)} + e^{j(-\psi_x/4 - \psi_y/2)} + e^{j(-3\psi_x/4 - \psi_y/2)}$$
$$+ e^{j(\psi_x/2 - \psi_y/4)} + e^{j(\psi_x/2 - 3\psi_y/4)} + e^{j(-\psi_x/2 + \psi_y/4)} + e^{j(-\psi_x/2 + 3\psi_y/4)}$$

$$(3)$$

$$\text{AF}_2 = e^{j(\psi_x/2 + \psi_y/4)} + e^{j(\psi_x/2 + 3\psi_y/4)} + e^{j(-\psi_x/2 - \psi_y/4)} + e^{j(-\psi_x/2 - 3\psi_y/4)}$$
$$+ e^{j(\psi_x/4 - \psi_y/2)} + e^{j(3\psi_x/4 - \psi_y/2)} + e^{j(-\psi_x/4 + \psi_y/2)} + e^{j(-3\psi_x/4 + \psi_y/2)}$$

$$(4)$$

where $\psi_x = kd \sin\theta \cos\varphi$, $\psi_y = kd \sin\theta \sin\varphi$, $k = 2\pi/\lambda$ is the wave number, d is the center distance of the adjacent same AMC element.

(a) Proposed structure   (b) Chessboard structure
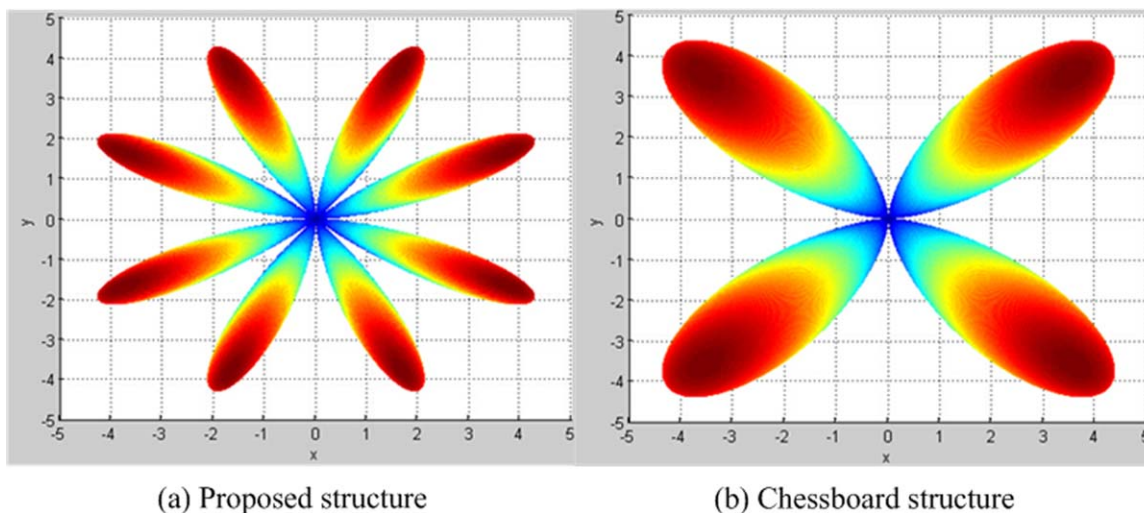
Figure 2 Two-dimensional plot of the scattered field for the proposed structure (a) and chessboard structure (b) with the same dimensions. [Color figure can be viewed in the online issue, which is available at wileyonlinelibrary.com]
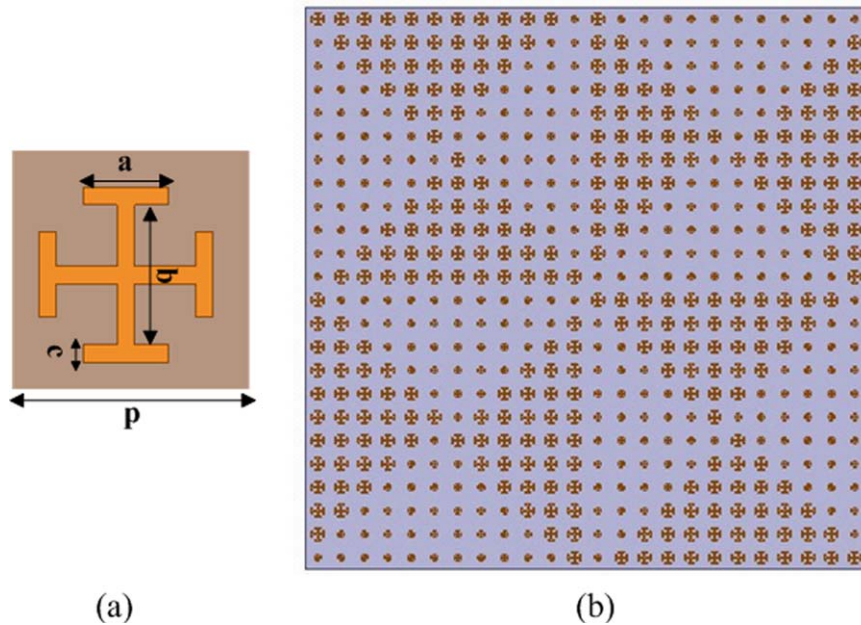
Figure 3 (a) Jerusalem Cross shaped structure unit, (b) combinatorial triangle-type structure based on Jerusalem Crosses. [Color figure can be viewed in the online issue, which is available at wileyonlinelibrary.com]

Considering that each element radiates the same amount of power ($A_1 = A_2$), the radiated field can be simplified as the following equation under normal incidence ($\theta = 0°$, $\varphi = 0°$):

$$\vec{E} = e^{j\varphi_1}\vec{E}_{\text{element}}\left(1 + e^{j(\varphi_2 - \varphi_1)}\right) \qquad (5)$$

It can be found from (5) that by tuning the phase difference in the range of $180° \pm 30°$, a good monostatic RCS reduction is achieved. Meanwhile, to obtain a wideband RCS reduction, we could make above phase difference range occur in the largest possible frequency band by adjusting the resonant frequencies of two AMC elements.

Due to the reallocation of array factors, the distribution of scattered field of the proposed structure should be different from the chessboard structure. This is demonstrated by two-dimensional plot of the scattered field for both structures with the same dimensions shown in Figure 2. As can be seen obviously in this figure, the power is mainly scattered in the diago-

nal direction for the chessboard structure. However, for the proposed combinatorial triangle-type structure, the power is decentralized and diffracted into more directions, making the attenuation of peak scattered field value possible, which will be further verified in the following section.

3. EXPERIMENTAL VERIFICATION AND DISCUSSION

To demonstrate the performance of the proposed combinatorial triangle-type configuration, the Jerusalem Cross shaped structure unit shown in Figure 3(a) is selected because it has no vias that can simplify the design and fabrication process. More importantly, the frequency response of this structure shows that the variation of the reflected wave phase at the operated frequency region is slower compared with other shaped structures [14], which is very helpful for wideband monostatic RCS reduction
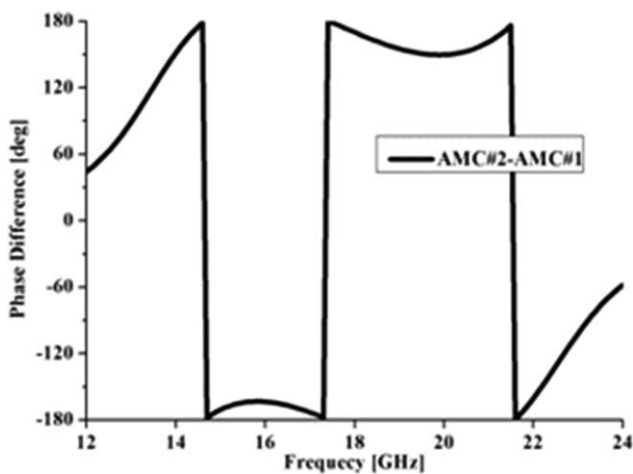
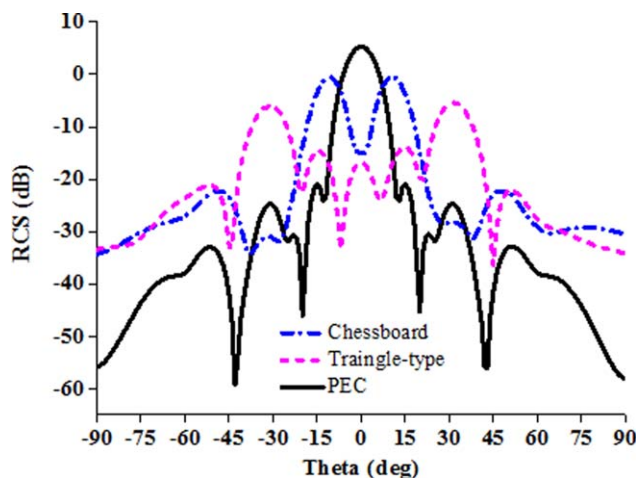**Figure 4** Reflected phase difference versus frequency between AMC #1 and AMC #2
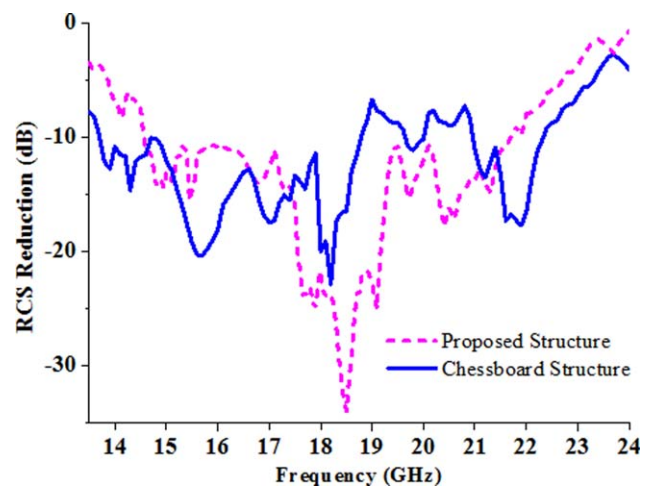
Figure 5 Monostatic RCS response of the combinatorial triangle-type configuration and chessboard configuration normalized by an equal size metallic plate. [Color figure can be viewed in the online issue, which is available at wileyonlinelibrary.com]
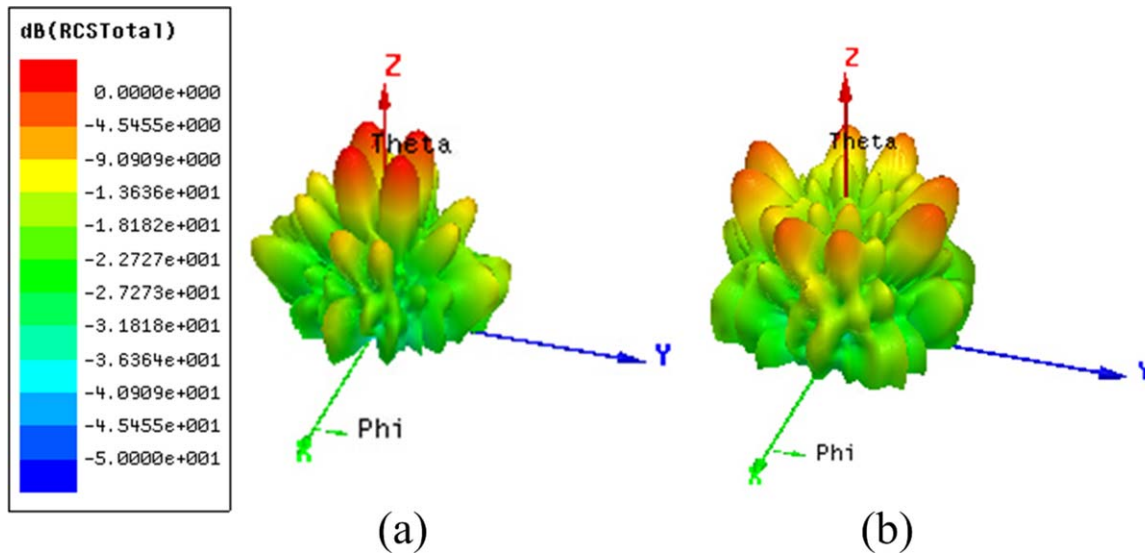
Figure 6 Scattered fields at 18.5 GHz of (a) the chessboard structure and (b) the combinatorial triangle-type structure. [Color figure can be viewed in the online issue, which is available at wileyonlinelibrary.com]

as described by (5). The proposed structure based on Jerusalem Crosses is depicted in Figure 3(b) and the Rogers 6010 substrate with a thickness of 1.27 mm and a dielectric constant of 10.2 is used in the simulation and fabrication.
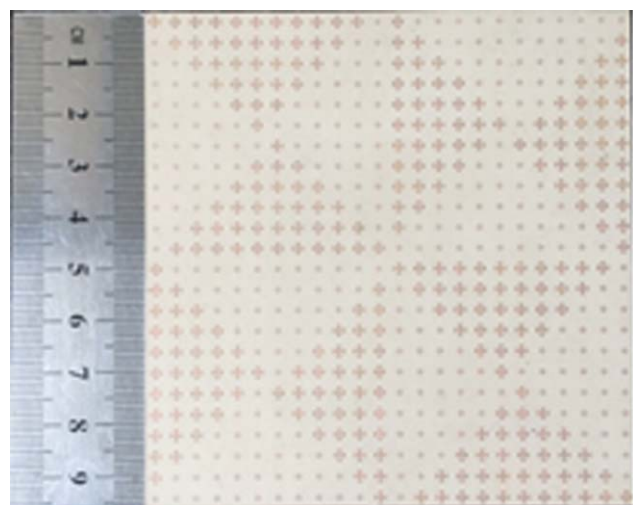
The AMC #1 and AMC #2 are simulated with the help of the full-wave solver Ansoft HFSS. The unitary cell model with appropriate periodic boundary condition is established to calculate the frequency band in which the periodic structure behaves as an AMC. The final optimized values of a, b, c for AMC #1 and AMC #2 are 1.06 mm, 1.74 mm, 0.22 mm, and 0.57 mm, 0.93 mm, 0.12 mm, respectively, and the period p is chosen to be 4.0 mm. The reflected phase difference between both AMC structures verse frequency is shown in Figure 4. It can be found that the phase difference in the range of $180° \pm 30°$ is from 14.3 to 22.1 GHz. Thus, a good monostatic RCS reduction can be expected in this wideband frequency region. To validate this behavior, the chessboard structure and the proposed combinatorial triangle-type structure with the same total dimension of 96 mm $\times$ 96 mm are simulated.

Figure 5 shows the monostatic RCS under normal incidence for the proposed triangle-type configuration and chessboard configuration, where the results are normalized by an equal size metallic plate. As can be seen in this figure, a wide bandwidth of nearly 10-dB RCS reduction is obtained from for both structures. The achieved RCS reduction bandwidth is in good agreement with the predicted bandwidth based on the $180° \pm 30°$ phase difference given in Figure 4. Moreover, it is worth mentioning that the RCS reduction of the proposed triangle-type structure is more obvious than the chessboard structure in most of the frequency band.

The scattered field of both structures at 18.5 GHz under normal incidence is presented in Figure 6. It can be clearly seen that the proposed structure has more grating lobes than the chessboard structure. Two cuts with the max scattered field of both structures are selected and shown in Figure 7 for better comparison. In phi = 45° cut of the chessboard structure, the power is mainly redirected to theta = $\pm 11°$ at the calculated frequency. While in phi = 17° cut of the proposed structure, the
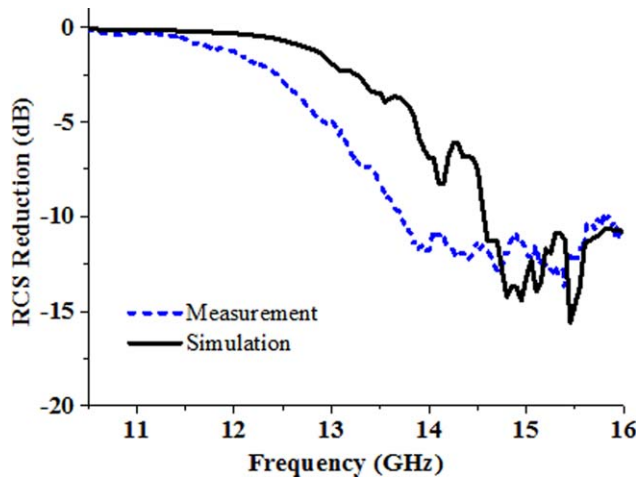

Figure 7 Bistatic RCS of the chessboard structure and combinatorial triangle-type structure at 18.5 GHz for phi cut with the max scattered field occurred. [Color figure can be viewed in the online issue, which is available at wileyonlinelibrary.com]

Figure 8 Photograph of the fabricated combinatorial triangle-type structure. [Color figure can be viewed in the online issue, which is available at wileyonlinelibrary.com]

Figure 9 Simulated and measured monostatic RCS of the combinatorial triangle-type AMC structure normalized by an equal size PEC plate. [Color figure can be viewed in the online issue, which is available at wileyonlinelibrary.com]

power is mainly concentrated on theta = ±31°. Meanwhile, there exists some grating lobes around theta = ±15°, ±55° with quite low value of the scattered field for the proposed structure, which is resulted from the reallocation of array factor as described in previous section. We could also find that peak value of the bistatic RCS of the PEC plate, the chessboard structure and the proposed structure are 5.53 dB, −0.52 dB, and −5 dB, respectively. Therefore, the peak scattered value is reduced by more than 5 dB compared with the chessboard structure.

Figure 8 depicts the photograph of the combinatorial triangle-type AMC structure. The fabricated structure is mounted in a vertical plane of the anechoic chamber and its monostatic behavior is evaluated through reflection coefficient characterization of the horn antenna. Due to the limited experimental condition, the test frequency can only be provided up to 16 GHz. The simulated and measured result of the monostatic RCS normalized by an equal size PEC plate is shown in Figure 9, where a good agreement is achieved between the simulation and measurement. It is found that the RCS reduction region is shifted to lower frequency in the measurement. This can be explained by that the operated frequency of AMC #1 and AMC #2 is changed for the fabricated structure due to the manufacturing error and the imperfect property of the used substrate.

4. CONCLUSION

A novel combinatorial triangle-type AMC structure for RCS reduction is presented in this article. A simplified model is developed to analyze the behavior of the proposed structure and the Jerusalem Cross shaped unit is used to demonstrate its performance. The simulated results show that the wideband monostatic RCS reduction of the proposed structure is obtained, and the peak value of scattered field is reduced more than 10 dB than the chessboard structure. Moreover, low bistatic RCS below −10 dB can be kept in a large angular domain from theta = −25° to 25°. Measurement of monostatic RCS of the fabricated triangle-type AMC structure is conducted and the discrepancy between simulation a d measurement is discussed.

REFERENCES

1. N. Engheta and R.W. Ziolkowski, Electromagnetic metamaterials: Physics and engineering explorations, Wiley-IEEE Press, New York, 2006.
2. F. Yang and Y. Rahmat-Samii, Microstrip antennas integrated with electromagnetic band-gap (EBG) structures: A low mutual coupling design for array applications, IEEE Trans Antennas Propag 51 (2003), 2936–2946.
3. M.E. de Cos, Y. Álvarez, and F. Las-Heras, Novel broadband artificial magnetic conductor with hexagonal unit cell, IEEE Antennas Wireless Propag Lett 10 (2011), 615–618.
4. D.J. Gregoire, C.R. White, and J.S. Colburn, A coaxial TEM cell for direct measurement of UHF artificial magnetic conductors, IEEE Antennas Propag Mag 54 (2012), 251–259.
5. A. Foroozesh and L. Shafai, Effects of artificial magnetic conductors in the design of low-profile high-gain planar antennas with high-permittivity dielectric superstrate, IEEE Antennas Wireless Propag Lett 8 (2009), 10–13.
6. M. Hosseinipanah and Q. Wu, Polarization-dependent artificial magnetic conductor structures using asymmetrical frequency selective surface, In: 3rd IEEE International Symposium on Microwave, Antenna, Propagation and EMC Technologies for Wireless Communications, Beijing, China, 2009, pp. 707–710.
7. Y.Q. Li, H. Zhang, Y.Q. Fu, and N.C. Yuan, RCS reduction of ridged waveguide slot antenna array using EBG radar absorbing material, IEEE Antennas Wireless Propag Lett 7 (2008), 473–476.
8. Y. Tan, N. Yuan, Y. Yang, and Y. Fu, Improved RCS and efficient waveguide slot antenna, Electron Lett 47 (2011), 582–583.
9. H.-Y. Xu, H. Zhang, K. Lu, and X.-F. Zeng, A holly-leaf-shaped monopole antenna with low RCS for UWB application, Prog Electromagn Res 117 (2011), 35–50.
10. Y. Zhang, R. Mittra, and B. Wang, Novel design for low-RCS screens using a combination of dual-AMC, In: Proceedings IEEE Antennas Propagation Society International Symposium, Charleston, SC, 2009, pp. 1–4.
11. M. Paquay and J.C. Iriarte, Thin AMC structure for radar cross-section reduction, IEEE Trans Antennas Propag 55 (2007), 3630–3637.
12. S. Simms and V. Fusco, Chessboard reflector for RCS reduction, Electron Lett 44 (2008), 316–317.
13. Y.L. Tsai and R.B. Hwang, RCS reduction of a composite AMC structure, In: 2011 IEEE International Workshop on Electromagnetics, Applications and Student Innovation (iWEM), Taibei, Taiwan, 2011, pp. 210–213.
14. J.C. Iriarte and A. Tellechea, Broadband radar cross-section reduction using AMC technology, IEEE Trans Antennas Propag 61 (2013), 6136–6143.

REDUCED SIZE OF SLOTTED-FRACTAL KOCH LOG-PERIODIC ANTENNA FOR 802.11af TVWS APPLICATION

Nur Akmal Abd. Rahman, Mohd Faizal Jamlos, Herwansyah Lago, Mohd Aminudin Jamlos, P. J. Soh, and Azremi Abdullah Al-Hadi
School of Computer and Communication Engineering, Advanced Communication Engineering Centre (ACE), Universiti Malaysia Perlis (UniMAP), Kampus Pauh Putra, Arau 02600, Perlis, Malaysia; Corresponding author: faizaljamlos@unimap.edu.my

ABSTRACT: *A reduced size of log-periodic fractal Koch antenna (LPFKA) design with rectangular slots for Television White Space Spectrum (TVWS) bands application is proposed in this letter. The new introduced design technique of tilted rectangular slots into the fractal Koch radiating elements found out to enhance the impedance bandwidth as well as realizing high gain and reducing the size of log-periodic antenna. The 10 LPFKA's radiating elements are located on both sides of the substrate in a crisscross arrangement and obtained 15.3% miniaturization as well as 50.79% bandwidth and maximum of 36% gain increment. The proposed antenna has a largest dimension of 305 × 280 mm², that is 0.44λ × 0.48λ over the lowest operating frequency of the 0.47–0.79 GHz TVWS bands. This antenna exhibits high gains of*